Vietnam Journal of Science and Technology ***55*** *(6A) (2017) 35-50*

CORROSION INHIBITION PERFOMANCE OF FOUR NATURAL THIAZOLE DERIVATIVES: QUANTUM CHEMICAL AND MONTE CARLO SIMULATION STUDIES

Duy Quang Dao[1, *], Thi Chinh Ngo[1], Nguyen Minh Thong[2], Pham Cam Nam[3]

[1]*Institute of Research and Development, Duy Tan University, 03 Quang Trung, Da Nang, Viet Nam*
[2]*The University of Danang, Campus in Kon Tum, 704 Phan Dinh Phung, Kon Tum, Viet Nam*
[3]*Department of Chemistry, University of Science and Technology - The University of Da Nang, 54 Nguyen Luong Bang, Lien Chieu, Da Nang, Viet Nam*

[*]Email: *daoduyquang@dtu.edu.vn*

Received: 15 June 2017; Accepted for publication: 21 December 2017

ABSTRACT

Some thiazole derivatives: 2-acetyl-thiazole, 2-isobutyl-thiazole, 4-methyl-5-(2-hydroxyethyl)-thiazole, 2,4,5-trimethyl-thiazole used as corrosion inhibitors for iron were calculated at DFT-PBEPBE/6-31+G(d,p) level of theory and by Monte Carlo simulations. Quantum chemical parameters such as EHOMO, ELUMO, and HOMO and LUMO energy gap, chemical potential (μ), electronegativity (χ), global hardness (η), softness (S), dipole moment and electrophilicity index (ω) have been calculated and discussed in detail to evaluate their inhibiting effectiveness. Mulliken-charges distribution and Fukui function were also calculated in order to visualize the reactive sites of the inhibitor molecules. Calculated results show that 2-acetyl-thiazole represents as the most efficient corrosion inhibitor. The –C4=C5– atomic center of thiazole ring demonstrates as the adsorption site in reaction with metallic surface. Corrosion inhibition effectiveness can be classified in decreasing order: ATZ > TMTZ ≈ SFR > ISTZ. Adsorption energies and interaction configurations of the four thiazole derivatives on Fe (110) were obtained using the Monte Carlo simulations. The results indicate that sulphur and nitrogen atoms as well as π-electronic systems within the thiazole ring aided the interaction between the inhibitor molecules and the Fe surface. All the four thiazole molecules adsorbed in parallel orientations on Fe (110) surface which ensures strong interactions with Fe. The adsorption energies were in accord with the results obtained using quantum chemical calculations.

Keywords: corrosion inhibitor, thiazole, DFT, Monte Carlo simulation, density functional theory

1. INTRODUCTION

Metal corrosion consists in an undesirable process which causes a progressive destruction by chemical reactions with different species available in corrosive medium. Understanding and solving this problem is a very attractive research field because it is related to a huge range of

industrial processes with million dollars [1]. Several technical solutions have been proposed such as electrochemical protection, use of corrosion inhibitor, metal coating protective technology, metal surface transformation, or non-metallic coating, etc. [2]. Among them, corrosion inhibitor is one of the most convenient and effective methods to protect metals from corrosion. In order to get better response to environmental regulations that are more and more severe, environmentally friendly (eco-friendly) corrosion inhibitors based on hetero-atomic organic compounds containing N, P, O or S have been recently preferred because of their strong chemical activity and low toxicity [3–6]. The inhibition efficiency of organic compounds is related to their adsorption properties. The adsorption mainly depends on some physical chemical properties of the molecule, such as its functional groups, steric effects, π-orbital character of donating electrons and electronic density of donor atoms [7,8], as well as on the possible interaction between π-orbitals of the inhibitor and d-orbitals of the metallic surface atoms [8]. The most popular parameters, which could use to evaluate the corrosion inhibition effectiveness of molecules, are the eigenvalues of highest-occupied molecular orbital (HOMO) and lowest-unoccupied molecular orbital (LUMO), HOMO–LUMO gap, electronegativity and chemical hardness, softness, dipole moment, etc. [9].

In recent times, molecular dynamics simulations are commonly used as an efficient tool to evaluate the interaction of corrosion inhibitor and metal surface [3,7,10–14], which plays a significant role in understanding the corrosion inhibition phenomena. This type of simulation provides more insights into the structure of the interface and how it differs from the bulk and the interaction of inhibitor molecules with metal surface [7, 15, 16].

Derivatives of thiazole (i.e. 1,3-thiazole) mainly possess a hetero-atomic ring, which contains one pyridine-like N-atom and one S-atom as present in thiophene and different substituents located at the C atom positions [17]. A number of thiazole derivatives are widely used as corrosion inhibitors with high efficiency for metal protection in industry. Research interest of several experimental and theoretical works in literature dedicated to this organic compound category, such as 1,3-thiazolidin-5-one derivatives [8], amino derivatives of 1,3-thiazole [7], 2-amino-4-(p-tolyl)-thiazole, 2-methoxy-1,3-thiazole and thiazole-4-carboxaldehyde [18], 2-aminothiazole [19], 2-amino-4-methyl-thiazole [20], 2-mercaptothiazoline [21], 2-aminothiazole derivatives [22], and other types of thiazole derivatives [23], etc. Whereas, to the best of our knowledge, there is no theoretical as well as experimental backgrounds have been systematically proposed to evaluate the corrosion inhibition performance of four compounds including 2-acetyl-thiazole (ATZ), 2-isobutyl-thiazole (ISTZ), 4-methyl-5-(2-hydroxyethyl)-thiazole (SFR) and 2,4,5-trimethyl-thiazole (TMTZ) (Fig. 1).

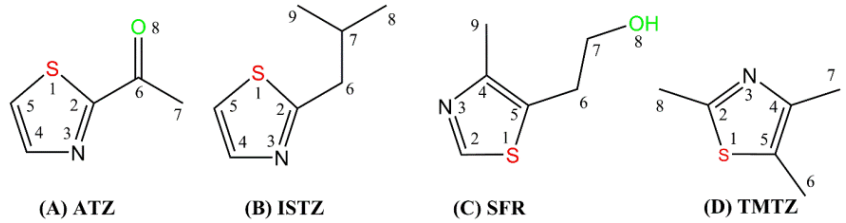

Figure 1. Molecular structures of studied thiazole derivatives: **(A)** 2-acetyl-thiazole (ATZ), **(B)** 2-isobutyl-thiazole (ISTZ), **(C)** 4-methyl-5-(2-hydroxyethyl)-thiazole (SFR), **(D)** 2,4,5-trimethyl-thiazole (TMTZ)

Thus, the goal of this paper is to evaluate the corrosion inhibition efficiency of four thiazole derivatives by using density functional theory (DFT) and Monte Carlo simulation tools. Several global quantum chemical parameters which help to compare the inhibitive effectiveness of the molecules were systematically calculated. The adsorption energy and the interaction mechanism of the inhibitors on the iron surface were also discussed based on the data of Monte Carlo simulations. Therefore, the obtained results will provide more theoretical information for designing novel inhibitors.

2. COMPUTATIONAL METHODS

2.1. Quantum chemical calculations

Geometry optimization and vibrational frequency calculations were carried out for both the neutral and protonated forms of corrosion inhibitors using DFT/PBEPBE method (correlation functional of Perdew, Burke and Ernzerhof) [24,25]. The 6-31+G(d,p), an appropriate basis set used in several studies on corrosion inhibitors such as thiadiazole and triazole derivatives, was chosen [26]. Zero-point energies (ZPEs) were obtained by frequency analysis and all minima were characterized to have zero imaginary frequency. The calculations were performed in the gas phase using Gaussian 09 program [27]. The energies of highest occupied molecular orbital (E_{HOMO}) and lowest unoccupied molecular orbital (E_{LUMO}) were calculated in detail for each inhibitor molecule.

According to DFT-Koopman's theorem [28], E_{HOMO} and E_{LUMO} allow defining vertical ionization potential (I) and electron affinity (A) as $I = -E_{HOMO}$ and $A = -E_{LUMO}$. For an N-electron system with total electronic energy (E) and an external potential $v(r)$, electronegativity (χ) is defined as the negative of chemical potential (μ) [5,29]:

$$\chi = -\mu = -\left(\frac{\partial E}{\partial N}\right)_{v(r)} \tag{1}$$

and hardness (η) is defined as [30]:

$$\eta = \frac{1}{2}\left(\frac{\partial \mu}{\partial N}\right)_{v(r)} = \frac{1}{2}\left(\frac{\partial^2 E}{\partial^2 N}\right)_{v(r)} \tag{2}$$

The absolute hardness and absolute electronegativity of inhibitors can be approximated on the basis of the finite difference approximation as follows [31]:

$$\eta = \frac{1}{2}(I - A) \tag{3}$$

$$\chi = \frac{1}{2}(I + A) \tag{4}$$

Global softness (S) is then defined as the reciprocal of absolute hardness [32]:

$$S = \frac{1}{\eta} = \left(\frac{\partial N}{\partial \mu}\right)_{v(r)} \tag{5}$$

The global electrophilicity index (ω) was introduced by Parr et al. [33] and it is given by the following equation:

$$\omega = \frac{\mu^2}{4\eta} \tag{6}$$

Dipole moment which is represented by a vector μ^*, is the most widely used quantity for describing the polarity of a given molecule [5]. The magnitude of dipole moment is product of charge on the atoms (q) and the distance between the two bonded atoms (R) by:

$$\mu^* = qR \tag{7}$$

Fukui function measuring reactivity in a local sense consists in the most important local reactivity index [5]. Atom condensed Fukui functions for nucleophilic (f^+) and electrophilic (f^-) attacks were calculated by applying the Mulliken population analysis and the finite difference approximations approach which were proposed by Yang and Mortier [34] as follows:

$$f_k^+ = \rho_{k(N+1)}(r) - \rho_{k(N)}(r) \tag{8}$$

$$f_k^- = \rho_{k(N)}(r) - \rho_{k(N-1)}(r) \tag{9}$$

where $\rho_{k(N+1)}$, $\rho_{k(N)}$, and $\rho_{k(N-1)}$ are the electron densities of the k^{th} atom in a molecule with (N + 1) electrons, N electrons and (N-1) electrons, respectively. Electron density values were approximated by Mulliken gross charges obtained from geometry optimizations [11]. Fukui functions, f^+ and f^- were calculated and visualized by Multiwfn software [35, 36].

2.2. Monte Carlo simulations

The interaction between the four natural thiazole derivatives and Fe (110) plane surface was carried out using Monte Carlo simulations. The adsorption locator code implemented in the Material Studio 7.0 software from Biovia-Accelrys Inc. USA was adopted in this simulation. The most stable Fe (110) crystal plane was used to mimic steel surface in this study. The Fe (110) surface was cleaved with a thickness of 5 Å. The cleaved plane was next enlarged to a (10 × 10) supercell. After that, a vacuum slab with 30 Å thickness was built above the Fe (110) plane to ensure that the non-bond calculations of the thiazole molecules do not interact with the periodic image of the bottom layer of atoms in the surface. The COMPASS (condensed phase optimized molecular potentials for atomistic simulation studies) force field was used for the simulation of all molecules and systems. In the work, four natural thiazole derivatives were simulated as corrosion inhibitor molecules on Fe (110) surface to locate the low energy adsorption sites and the nature of adsorption configurations.

3. RESULTS AND DISCUSSION

3.1. Neutral species

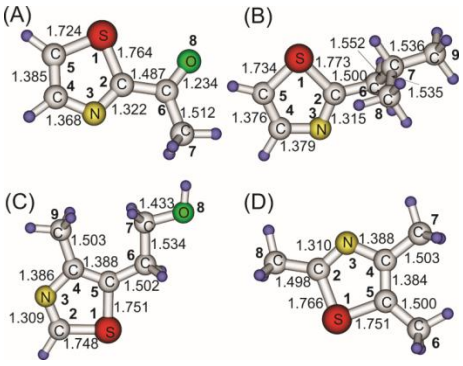

Figure 2. Gas phase optimized geometry of the neutral form of **(A)** ATZ, **(B)** ISTZ, **(C)** SFR and **(D)** TMTZ at the PBEPBE/6-31+G(d,p) level of theory

The optimized geometry accompanied with numbered atomic sites and bond lengths in Å for the neutral form of ATZ, ISTZ, SFR and TMTZ calculated at the PBEPBE/6-31+G(d,p) level of theory in the gas phase is displayed in Fig. 2.

It can be observed in Fig. 2 that the bond lengths of thiazole rings of four studied thiazole derivatives are slightly different. Indeed, the length of S1–C2 bond of these molecules increase in the following order: SFR < ATZ < TMTZ < ISTZ corresponding to values of 1.748, 1.764, 1.766 and 1.773 Å, respectively. The C2–N3 bond lengths increase in the sequence: SFR < TMTZ < ISTZ < ATZ with the values of 1.309, 1.310, 1.315 and 1.322 Å, respectively. Similarly, the length values equal to 1.368, 1.379, 1.386 and 1.388 Å are recorded according to the N3–C4 bonds of ATZ, ISTZ, SFR and TMTZ, respectively. As all C2=N3 bond lengths are shorter than the ones of a C–N single bond (i.e. 1.39 – 1.40 Å) [37], this allows confirming the existence of C2=N3 double bond. The C4=C5 bond lengths of four thiazole derivatives vary from 1.376 to 1.388 Å that also confirms a presence of localized double bond. On the other hand, the bond angles within the ring of four thiazole derivatives are quasi-similar (as shown in Fig. 2). For example, the C2–S1–C5 angles are 88.41, 89.26, 89.16 and 89.64° corresponding to ATZ, ISTZ, SFR and TMTZ, respectively. The C2–N3–C4 angles are equal to 110.69, 111.42, 111.13 and 112.19°, and the C4–C5–S1 angles of ATZ, ISTZ, SFR and TMTZ equal to 110.62, 109.65, 109.11 and 109.00°, respectively. Moreover, dihedral angles within the thiazole ring are all equal to 0°. This allows confirming the perfect planarity of the studied molecules which is one of the most important conditions for a good adsorption of inhibitor on metal surface. The slight difference of optimized geometrical parameters results from the effect of $–CH_3CO$, $–CH_2CH(CH_3)_2$, $–CH_3$ and $–(CH_2)_2OH$ substituent groups at the C atom position within the thiazole ring.

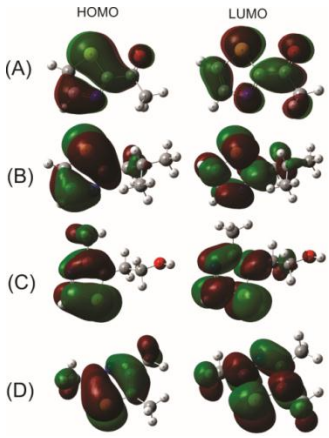

Figure 3. HOMO and LUMO of **(A)** ATZ, **(B)** ISTZ, **(C)** SFR and **(D)** TMTZ at the PBEPBE/6-31+G(d,p) level of theory for the neutral species in the gas phase

The frontier molecular orbitals are the most important parameters which allow analyzing the molecular reactivity. The HOMO and LUMO of four studied thiazole derivatives are presented in Fig. 3. As can be seen in Fig. 3, the frontier molecular orbitals are spread entire the studied molecular systems, especially within the thiazole ring. This observation results from the high electron densities of the –C5=C4–N3– and –S1–C2– groups of the thiazole ring. Strong electron delocalization can be found over these two atomic groups. Thus, a plat or parallel adsorption of the inhibitors which tends to a strong interaction with metal surface and a high efficiency of corrosion inhibition can be suggested [37]. This will be confirmed by Monte Carlo simulations presented in the next section.

Quantum chemical parameters related to the reactivity of the thiazole derivative based-corrosion inhibitors (i.e. ATZ, ISTZ, SFR and TMTZ) are resumed in Table 1. The parameters

include HOMO energy (E_{HOMO}), LUMO energy (E_{LUMO}), energy gap between HOMO and LUMO ($\Delta E_{L-H} = E_{LUMO} - E_{HOMO}$), ionization potential (I), electron affinity (A), chemical potential (μ), electronegativity (χ), global hardness (η), softness (S), dipole moment and electrophilicity index (ω).

Table 1. Quantum chemical parameters of the neutral form of ATZ, ISTZ, SFR and TMTZ calculated at the PBEPBE/6-31+G(d,p) level in the gas phase.

Parameter	**ATZ**	**ISTZ**	**SFR**	**TMTZ**
E_{HOMO} (eV)	-7.72	-7.47	-7.46	-7.27
E_{LUMO} (eV)	-4.60	-2.48	-3.10	-3.07
ΔE_{L-H} (eV)	3.12	4.99	4.36	4.21
Ionization potential (I) (eV)	7.72	7.47	7.46	7.27
Electron affinity (A) (eV)	4.60	2.48	3.10	3.07
Chemical potential (μ)	-6.16	-4.98	-5.28	-5.17
Electronegativity (χ) (eV)	6.16	4.98	5.28	5.17
Hardness (η) (eV)	1.56	2.50	2.18	2.10
Softness (S) (eV^{-1})	0.64	0.40	0.46	0.48
Dipole (Debye)	2.86	1.25	1.84	1.19
Electrophilicity index (ω)	6.08	2.48	3.20	3.18

Several authors confirmed that E_{HOMO} is well related to the corrosion inhibition efficiency [3, 5, 38] and E_{HOMO} is often associated with the electron-donating ability of an inhibitor molecule. The adsorption of an inhibitor on protected metal surface occurs via donor-acceptor interaction between the π-electrons of heterocyclic compound and the vacant d-orbitals of the metal atoms [5]. Thus, a higher E_{HOMO} value indicates a better electrons donating tendency of inhibitor to an acceptor metal molecule. And this results in higher adsorption and better inhibition efficiency. It can be confirmed from Table 1 that the electron donating capacity of the four thiazole derivatives is in the order: ATZ < ISTZ ≈ SFR < TMTZ corresponding to E_{HOMO} value of –7.72, –7.47, –7.46 and –7.27 eV, respectively.

Inversely, E_{LUMO} indicates the electron-accepting capacity of an inhibitor molecule. It means that the lower E_{LUMO} is, the higher is the electron accepting ability of that molecule. Thus, the electron accepting capacity of four potential inhibitors is in the order: ATZ > SFR ≈ TMTZ > ISTZ with E_{LUMO} values of –4.60, –3.10, –3.07 and –2.48 eV, respectively (Table 1).

Energy gap, ΔE_{L-H}, represents the reactive tendency of an inhibitor molecule towards the protected metal surface. Generally, a low energy gap organic molecule is more polarized and associated with high chemical reactivity and low kinetic stability [5, 37, 39]. For that reason, a low ΔE_{L-H} results in a high reactivity of molecule and in an increase of the strength of adsorption and hence in inhibition efficiency. Thus, based on energy of the frontier orbitals, the inhibition efficiency of four studied thiazole derivatives follows order: ATZ > TMTZ ≈ SFR > ISTZ corresponding to values of 3.12, 4.21, 4.36 and 4.99 eV, respectively.

Electronegativity (χ) which is the negative of the chemical potential (μ), also describes the tendency of a molecule (i.e. inhibitor molecule or metallic surface) to attract electrons (or electron density) towards itself [5]. So the higher the electronegativity is, the stronger a molecule attracts electron towards it. As can be observed in Table 1, the electronegativity of four studied thiazole compounds follows the order: ATZ > SFR ≈ TMTZ > ISTZ corresponding to values of 6.16, 5.28, 5.17 and 4.98 eV, respectively.

Chemical hardness (η) and softness (S) are important quantum properties that measure the reactivity and stability of an inhibitor molecule. Softness which is the inverse of chemical hardness, is also an indicator of polarizability of molecules [3]. A soft molecule is more reactive than a hard molecule because of its easier electron offering capacity. The corrosion inhibitor and the metal surface are both considered as a soft base and a soft acid, respectively. According to the softness values (S) reported in Table 1, this property follows the tendency: ATZ > TMTZ > SFR > ISTZ with S values of 0.64, 0.48, 0.46 and 0.40 eV^{-1}, respectively. This result allows confirming the decreasing order of inhibition efficiency as follows: ATZ > TMTZ ≈ SFR > ISTZ.

Dipole moment is widely used to characterize the polarity of a molecule [5,11]. There are dissenting opinions in the use of dipole moment as a descriptor for inhibition efficiency [11]. Some authors reported that the inhibition performance increases with decreasing dipole moment of inhibitor [40]. Some others believe that high dipole moment enhances inhibition efficiency due to increased dipole – dipole interaction between the inhibitor molecules and metallic surface system [41,42]. For the four studied thiazole molecules, the dipole moment is arranged in the trend: ATZ > SFR > ISTZ > TMTZ corresponding to values of 2.86, 1.84, 1.25 and 1.19 Debye, respectively (Table 1). So the results of the actual study seem to support to the second suggestion.

Finally, electrophilicity index (ω) denotes the electron accepting capacity of an inhibitor molecule [5]. This property follows in decreasing order: ATZ > SFR ≈ TMTZ > ISTZ corresponding to values of 6.08, 3.20, 3.18 and 2.48, respectively. This observation allows confirming that ATZ has the highest ability to accept electron from the metallic surface compared with the other three inhibitor molecules. This result is fully coherent with the E_{LUMO} trend.

Table 2 resumes the calculated Mulliken charges for the neutral form of ATZ, ISTZ, SFR and TMTZ at the PBEPBE/6-31+G(d,p) level in the gas phase.

Mulliken population analysis has been widely accepted as an identification of adsorption centers of inhibitors [5,43,44]. And it is reported that the highest negative charge atom has the highest tendency to donate electron to metallic surface [45]. Thus, the inhibitor molecule is likely to interact with the metallic surface through such atomic positions. As can be seen in Table 2, the N3 hetero-atom of the studied thiazole derivatives has weak negative charge (i.e. -0.058, -0.029, -0.031 and -0.027 for ATZ, ISTZ, SFR and TMTZ, respectively). The highest negative charge is found at the C atom position of the substitution, for example at C7 of ATZ (i.e. -0.689), at C6 of ISTZ (i.e. -0.863), at C9 of SFR (i.e. -0.866) and at C7 of TMTZ (i.e. -0.839). This observation results from the electron donating property of the methyl groups. Moreover, the heteroatom S1 of studied inhibitor molecules and some C atoms (i.e. C6 atom of ATZ, C7 of ISTZ, and C5 of SFR and TMTZ) possess strong positive charge. So these atomic positions could inversely accept electrons from the surface metal.

Table 2. Mulliken charges for the neutral form of ATZ, ISTZ, SFR and TMTZ calculated at the PBEPBE/6-31+G(d,p) level in the gas phase.

Atoms	**ATZ**	**ISTZ**	**SFR**	**TMTZ**
S1	0.321	0.240	0.240	0.133
C2	-0.262	0.051	-0.083	0.098
N3	-0.058	-0.029	-0.031	-0.027
C4	-0.128	-0.101	-0.175	-0.305
C5	-0.100	-0.185	0.566	0.684
C6	0.364	-0.863	-0.648	-0.682
C7	-0.689	0.349	-0.265	-0.839
C8	-	-0.635	-	-0.723
C9	-	-0.726	-0.866	-
O8	-0.402	-	-0.485	-

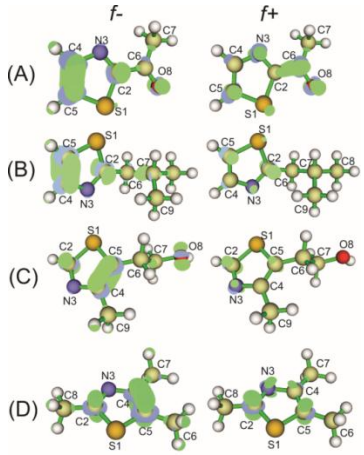

Figure 4. Fukui functions for the neutral form of **(A)** ATZ, **(B)** ISTZ, **(C)** SFR and **(D)** TMTZ visualized at 0.006 isosurfaces

Fukui functions measure the chemical reactivity as well as provide information about the reactive regions and the electrophilic active site (f^+) and nucleophilic one (f^-) of organic inhibitors. Generally, atomic sites with important values of f^+ tend to receive charges from a charged metallic surface, while sites with substantial values of *f-* have tendencies to donate charges to metal surface [11]. Fukui functions for the neutral form of ATZ, ISTZ, SFR and TMTZ calculated and visualized at 0.006 isosurfaces by Multiwfn code [35,36] are shown in Fig. 4. As can be seen in Fig. 4, all four thiazole derivatives have several electrophilic and nucleophilic active sites which could facilitate their adsorption onto the metallic surface. Atoms in thiazole ring, especially C4, C5 and C2 sites at which the largest *f-* are found, consist in nucleophilic sites, while the N3, C5 as well as C2 atoms are electrophilic sites with the largest *f*+.

3.2. Protonated species

The studied thiazole derivatives were singly protonated at the position of N3, S1 and O8 atoms. The most preferred protonation site in each molecule was determined on the basis of gas proton affinity (PA) and gas basicity (GB). Each inhibitor was treated as a potential base with

one prospective basic site [11]. Thus, the protonation of a neutral basic compound B at a specific donor site is written as follows:

$$B + H^+ \rightleftharpoons BH^+ \tag{10}$$

The PA can be calculated from Eq. (10) as the negative value of difference in enthalpies of product and reactants as follows [46–48]:

$$PA = -\Delta H = -\left[H_{gas}(BH^+) - \left(H_{gas}(B) + H_{gas}(H^+)\right)\right] \tag{11}$$

where H_{gas} is the enthalpy at 298.15 K. The enthalpy in gas phase of a proton $H_{gas}(H^+)$ is equal to its translational energy (3/2RT = 3.720 kJ/mol).

Gas phase basicity (GB) of each protonated site was calculated as the negative value of change in Gibbs free energy of the protonation reaction (Eq. 10) as follows [49]:

$$GB = -\Delta G = -\left[G_{gas}(BH^+) - \left(G_{gas}(B) + G_{gas}(H^+)\right)\right] \tag{12}$$

where G_{gas} is free energy at 298.15 K. The $G_{gas}(H^+)$ is calculated as:

$$G_{gas}(H^+) = {}^3/_2\, RT + TS(H^+) \tag{13}$$

where $S(H^+)$ is taken to be 108.95 J/mol.K [49].

Absolute values of PA and GB and their relative values (ΔPA and ΔGB) calculated at 298.15 K by using the DFT-PBEPBE/6-31+G(d,p) are listed in Table 3. The results show that the most stable protonated site within the four thiazole derivatives is N3 atom of thiazole ring. On the other hand, there is no chance of multiple protonation for all the studied inhibitors when ΔPA and ΔGB values are all far from that of the most preferred site of protonation. For example, the ΔPA and ΔGB values of S1 position are respectively -184.22 and -181.27 kJ/mol for ATZ, -196.02 and -193.81 kJ/mol for ISTZ, -203.91 and -203.61 kJ/mol for SFR and -190.45 and -192.81 kJ/mol for TMTZ. The similar results are observed for O8 atomic site.

Table 3. Relative values of proton affinity (PA) and gas basicity (GB) for ATZ, ISTZ, SFR and TMTZ calculated at the PBEPBE/6-31+G(d,p) level in the gas phase.

Compounds	**ATZ**			**ISTZ**		**SFR**			**TMTZ**	
Protonation site	N3	O8	S1	N3	S1	N3	O8	S1	N3	S1
PA (kJ/mol)	869.69	833.64	685.47	930.04	734.03	928.35	773.48	724.44	948.86	758.42
GB (kJ/mol)	899.23	865.09	717.96	959.21	765.40	958.49	804.51	754.88	980.28	787.47
ΔPA*	0	-36.05	-184.22	0	-196.02	0	-154.88	-203.91	0	-190.45
ΔGB**	0	-34.14	-181.27	0	-193.81	0	-153.98	-203.61	0	-192.81
∗ ΔPA = PA(less stable) – PA(most stable); ** ΔGB = GB(less stable) – GB(most stable)										

The bond lengths in Å of the optimized geometry for the most stable protonated form of four thiazole derivatives at PBEPBE/6-31+G(d,p) level of theory in the gas phase are presented in Fig. 5. And Fig. 6 allows to visualize HOMO and LUMO of the protonated molecules ATZ, ISTZ, SFR and TMTZ at the PBEPBE/6-31+G(d,p) level of theory in the gas phase, and related quantum chemical parameters are all listed in Table 4.

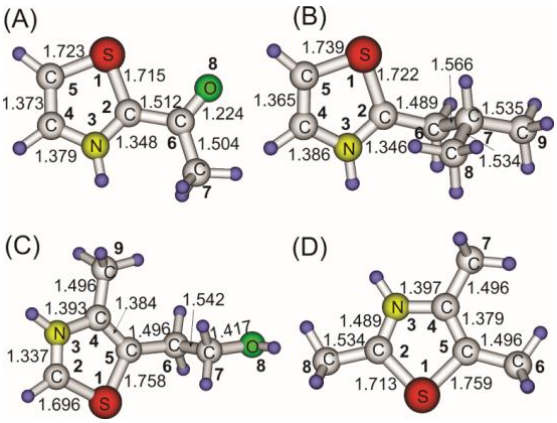

Figure 5. Gas phase optimized geometry of the most stable protonated form of **(A)** ATZ **(B)** ISTZ at N3 atom, **(C)** SFR and **(D)** TMTZ at the PBEPBE/6-31+G(d,p) level of theory.

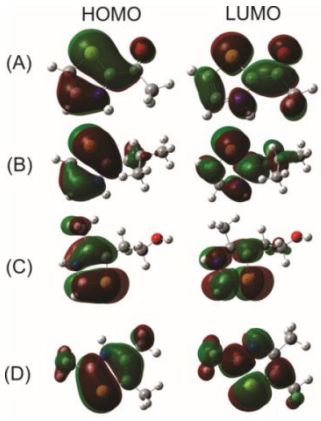

Figure 6. HOMO and LUMO for the most stable protonated species of **(A)** ATZ, **(B)** ISTZ, **(C)** SFR and **(D)** TMTZ at the PBEPBE/6-31+G(d,p) level of theory in the gas phase.

Table 4. Quantum chemical parameters of the protonated form of ATZ, ISTZ, SFR and TMTZ calculated at the PBEPBE/6-31+G(d,p) level in the gas phase.

Parameter	**ATZ-NH**	**ISTZ-NH**	**SFR-NH**	**TMTZ-NH**
E_{HOMO} (eV)	-7.91	-7.71	-7.73	-7.53
E_{LUMO} (eV)	-4.65	-3.27	-3.23	-3.15
ΔE_{L-H} (eV)	3.26	4.44	4.50	4.38
Ionization potential (I) (eV)	7.91	7.71	7.73	7.53
Electron affinity (A) (eV)	4.65	3.27	3.23	3.15
Chemical potential (μ)	-6.28	-5.49	-5.48	-5.34
Electronegativity (χ) (eV)	6.28	5.49	5.48	5.34
Hardness (η) (eV)	1.63	2.22	2.25	2.19
Softness (S) (1/eV)	0.61	0.45	0.44	0.46
Dipole (Debye)	6.10	4.11	6.16	2.54
Electrophilicity index (ω)	6.04	3.40	3.33	3.26

It can be seen that there are considerable changes in all the calculated quantum parameters, bond lengths as well as charge distribution entire the molecules (Table 5). The results in Table 4 show that ATZ-NH has the lowest ΔE_{L-H} (i.e. 3.26 eV) while the other three inhibitors have similar ΔE_{L-H} values with a difference from 0.06 to 0.12 eV. This trend of the protonated form is coherent with the one of the neutral form, and this supports to ATZ as the most efficient inhibitor among four thiazole compounds. The ATZ-NH has also the least chemical hardness (η) (i.e. 1.63 eV compared with 2.19, 2.22 and 2.25 of TMTZ-NH, ISTZ-NH and SFR-NH, respectively) which confirms its highest chemical reactivity and enhances its inhibition efficiency. Moreover, the dipole moment of the protonated inhibitors is sharply higher than the

one of their neutral form with the difference from 1.36 Debye (for TMTZ) to 4.32 Debye (for SFR). The dipole moment values of the thiazole molecules are in order: ATZ-NH ≈ SFR-NH > ISTZ-NH > TMTZ-NH. It means that the protonation tends to a stronger polarizability of the organic inhibitors, and so results in better adsorption onto the metallic surface. Finally, the electrophilicity value (ω) of ATZ-NH is also the highest compared with the one of others species. And the order of ω is ATZ-NH > ISTZ-NH ≈ SFR-NH ≈ TMTZ-NH corresponding to values of 6.04, 3.40, 3.33 and 3.26, respectively.

Table 5. Mulliken charges for the protonated form of ATZ, ISTZ, SFR and TMTZ calculated at the PBEPBE/6-31+G(d,p) level in the gas phase

Atoms	**ATZ-NH**	**ISTZ-NH**	**SFR-NH**	**TMTZ-NH**
S1	0.589	0.553	0.517	0.439
C2	-0.150	0.216	-0.109	-0.044
N3	-0.085	-0.084	-0.064	-0.052
C4	-0.129	-0.176	-0.120	-0.339
C5	-0.043	-0.027	0.624	0.696
C6	0.291	-1.064	-0.777	-0.575
C7	-0.700	0.310	-0.219	-0.812
C8	-	-0.595	-	-0.656
C9	-	-0.697	-0.791	-
O8	-0.316	-	-0.466	-

The Mulliken-charges distribution entire the protonated inhibitors are not considerably different compared with the ones of the neutral species. For example, the highest negative charges are always found at the C7 position of ATZ-NH (i.e. -0.700) and TMTZ-NH (i.e. -0.812) and at C6 for ISTZ-NH (-1.064) and at C9 for SFR-NH (-0.791). Moreover, the highest positive charges are observed at C5 atom for SFR-NH and TMTZ-NH (i.e. 0.624 and 0.696, respectively) which is similar with the case of the neutral species of the inhibitors. However, for ATZ-NH and ISTZ-NH the highest positive charge is situated at S1 atom (with the charge of 0.589 for ATZ-NH and of 0.553 for ISTZ-NH). And it is observed that the protonation at N3 atom of thiazole ring tends to strongly increase the positive charge of the S1 atom (Table 5).

Figure 7 represents Fukui functions for the most stable protonated form of ATZ-NH, ISTZ-NH, SFR-NH and TMTZ-NH visualized at 0.006 isosurfaces for both the electrophilic active site (f^+) and nucleophilic one (f^-). As can be seen in Fig. 7, C2, C4 and C5 atoms within the thiazole ring of the protonated species play as the most important nucleophilic sites. Furthermore, O8 atoms present in ATZ-NH and SFR-NH are also nucleophilic which is observed in the case of the neutral thiazole species. Thus these atoms have strong tendency to donate electrons towards the metallic surface. On the other hand, S1, N3, and C2 atoms within the thiazole ring are expressed as the largest electrophilic positions which tend to receive electron from the metallic surface.

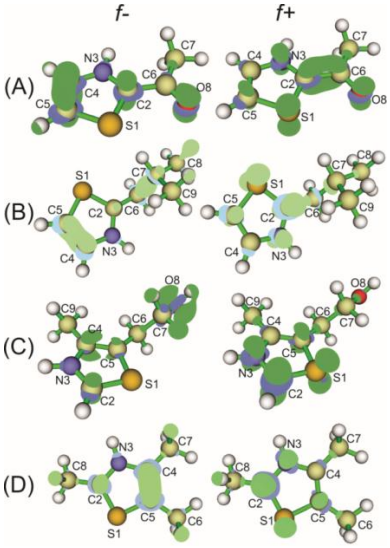

Figure 7. Fukui functions for the protonated form of **(A)** ATZ-NH, **(B)** ISTZ-NH, **(C)** SFR-NH and **(D)** TMTZ-NH visualized at 0.006 isosurfaces for f^+ and f^-.

3.2. Monte Carlo simulations results

Energetic parameters including the total energy, adsorption energy, rigid adsorption and deformation energies derived from Monte Carlo simulations for the four natural thiazole derivatives are listed in Table 6. The adsorption energy is attributed to the energy released during the relaxed adsorbate components adsorbed on the substrate. The adsorption energy is the addition of rigid adsorption and deformation energies of the adsorbate component. Higher negative adsorption energy values indicate a more stabilized and stronger interaction between a metal and an inhibitor molecule[16,50]. It can be seen from the results in Table 6 that the adsorption energies of the four natural thiazole derivatives investigated followed the order: ATZ > TMTZ ≈ SFR > ISTZ. This order is the same obtained by quantum chemical calculations. All the molecules simulated adsorbed totally in a parallel at manner on Fe, which enhances its surface coverage as it interact with the steel surface (Fig. 8).

Table 6. Outputs and descriptors calculated by Monte Carlo simulation for adsorption of four natural thiazole derivatives on Fe (110) surface in the gas phase (in kcal/mol).

Systems	Total energy	Adsorption energy	Rigid adsorption energy	Deformation energy	dEad/dNi: Inhibitor
Fe(110) + ATZ	-69.782	-73.780	-75.601	1.820	-73.780
Fe(110) + TMTZ	-70.268	-72.220	-74.432	2.211	-72.220
Fe(110) + SFR	-71.014	-72.166	-72.573	0.406	-72.166
Fe(110) + ISTZ	-49.097	-66.954	-67.578	0.624	-66.954

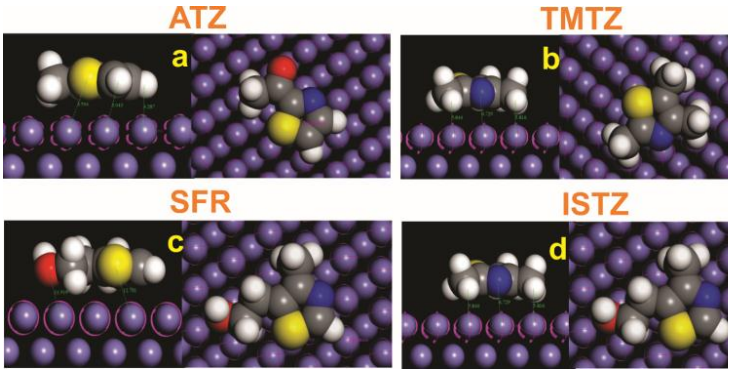

Figure 8. Top and side views of equilibrium adsorption configurations of (**A**) ATZ, (**B**) TMTZ (**C**) SFR and (**D**) ISTZ obtained using Monte Carlo simulations in the gas phase

4. CONCLUSIONS

Density functional theory at the PBEPBE/6-31+G(d,p) level of theory and Monte Carlo simulations were performed to study the inhibition efficiency and the adsorption mechanisms of four thiazole derivatives (ATZ, ISTZ, SFR and TMTZ) used as corrosion inhibitors for iron. The chemical quantum parameters of the neutral species and the protonated ones are calculated in detail. The conclusions drawn from this study are multiple:

1. The four studied thiazole derivatives have a perfect planarity of the thiazole ring, this ensure the good covering of these inhibitors on the metal surface in corrosion process.

2. The HOMO and LUMO are strongly delocalized on the thiazole ring. This observation results from the high electron densities of the –C4=C5–N3– and –S1–C2– atomic groups within the thiazole ring which favor the nucleophile and electrophile attacks in the reaction between the inhibitor molecules and the Fe surface.

3. Regarding to all quantum chemical parameters, ATZ in both the neutral and protonated forms represents as the most efficient corrosion inhibitor by compared with the other three thiazole derivatives, i.e. ISTZ, SFR and TMTZ. And the corrosion inhibition effectiveness can be classified in decreasing order: ATZ > TMTZ ≈ SFR > ISTZ.

4. The Mulliken population and Fukui functions indicate that the –C4=C5– atomic centers consist in the main adsorption sites.

5. Monte Carlo simulations indicate high negative adsorption energies of interaction between the inhibitors and Fe. All the thiazole molecules investigated were adsorbed in parallel orientations on the Fe surface indicating a strong interaction. The ranking of the adsorption energies of the four molecules using this computational approach are similar to the obtained results using quantum chemical calculations.

Acknowledgements. This research is funded by Vietnam National Foundation for Science and Technology Development (NAFOSTED) under grant number 104.06-2015.09.

REFERENCES

1. Cruz J., Garcia-Ochoa E., Castro M. - Experimental and Theoretical Study of the 3-Amino-1,2,4-triazole and 2-Aminothiazole Corrosion Inhibitors in Carbon Steel, J. Electrochem. Soc. **150** (2003) B26.
2. Cruz J., Martínez R., Genesca J., García-Ochoa E. - Experimental and theoretical study of

1-(2-ethylamino)-2-methylimidazoline as an inhibitor of carbon steel corrosion in acid media, J. Electroanal. Chem. **566** (2004) 111–121.

3. Kaya E., Tüzün B., Kaya C., Obot I.B. - Determination of corrosion inhibition effects of amino acids: Quantum chemical and molecular dynamic simulation study, J. Taiwan Inst. Chem. Eng. **58** (2016) 528–535.
4. Donnelly B., Downie T.C., Grzeskowiak R., Hamburg H.R., Short D. - The effect of electronic delocalization in organic groups R in substituted thiocarbamoyl $RCSNH_2$ and related compounds on inhibition efficiency, Corros. Sci. **18** (1978) 109–116.
5. Obot I.B., Macdonald D.D., Gasem Z.M. - Density functional theory (DFT) as a powerful tool for designing new organic corrosion inhibitors. Part 1: An overview, Corros. Sci. **99** (2015) 1–30.
6. Ansari K. R., Quraishi M.A. - Experimental and computational studies of naphthyridine derivatives as corrosion inhibitor for N80 steel in 15% hydrochloric acid, Phys. E Low-Dimensional Syst. Nanostructures. **69** (2015) 322–331.
7. Guo L., Renv, Zhouv, Xu S., Gong Y., Zhang S. - Theoretical evaluation of the corrosion inhibition performance of 1,3-thiazole and its amino derivatives, Arab. J. Chem. **10** (2017) 121-130.
8. Al-Sarawy A.A., Fouda A.S., El-Dein W.A.S. - Some thiazole derivatives as corrosion inhibitors for carbon steel in acidic medium, Desalination. **229** (2008) 279–293.
9. Olasunkanmi L.O., Kabanda M.M., Ebenso E.E. - Quinoxaline derivatives as corrosion inhibitors for mild steel in hydrochloric acid medium: Electrochemical and quantum chemical studies, Phys. E Low-Dimensional Syst. Nanostructures. **76** (2016) 109–126.
10. Obot I.B., Umoren S.A., Gasem Z.M., Suleiman R., El Ali B. - Theoretical prediction and electrochemical evaluation of vinylimidazole and allylimidazole as corrosion inhibitors for mild steel in 1M HCl, J. Ind. Eng. Chem. **21** (2015) 1328–1339.
11. Olasunkanmi L.O., Obot I.B., Kabanda M.M., Ebenso E.E. - Some Quinoxalin-6-yl Derivatives as Corrosion Inhibitors for Mild Steel in Hydrochloric Acid: Experimental and Theoretical Studies, J. Phys. Chem. C. **119** (2015) 16004–16019.
12. Sasikumar Y., Adekunle A.S., Olasunkanmi L.O., Bahadur I., Baskar R., Kabanda M.M., et al. - Experimental, quantum chemical and Monte Carlo simulation studies on the corrosion inhibition of some alkyl imidazolium ionic liquids containing tetrafluoroborate anion on mild steel in acidic medium, J. Mol. Liq. **211** (2015) 105–118.
13. Tang Y., Yang X., Yang W., Chen Y., Wan R. - Experimental and molecular dynamics studies on corrosion inhibition of mild steel by 2-amino-5-phenyl-1,3,4-thiadiazole, Corros. Sci. **52** (2010) 242–249.
14. Obot I.B., Gasem Z.M., Umoren S.A. - Understanding the Mechanism of 2-mercaptobenzimidazole Adsorption on Fe (110), Cu (111) and Al (111) Surfaces : DFT and Molecular Dynamics Simulations Approaches, Int. J. Electrochem. Sci. **9** (2014) 2367–2378.
15. Saha S.K., Ghosh P., Hens A., Murmu N.C., Banerjee P. - Density functional theory and molecular dynamics simulation study on corrosion inhibition performance of mild steel by mercapto-quinoline Schiff base corrosion inhibitor, Phys. E Low-Dimensional Syst. Nanostructures. **66** (2015) 332–341.
16. Obot I.B., Kaya S., Kaya C., Tüzün B. - Density Functional Theory (DFT) modeling and Monte Carlo simulation assessment of inhibition performance of some carbohydrazide Schiff bases for steel corrosion, Phys. E Low-Dimensional Syst. Nanostructures. **80**

(2016) 82–90.

17. Eicher T., Hauptmann S., Speicher A. - The Chemistry of Heterocycles, Wiley-VCH Verlag GmbH & Co. KGaA, Weinheim, FRG, 2003. doi:10.1002/352760183X.
18. Amin M.A., Saracoglu M., Kandemirli F., Amin M.A., Vurdu C.D., Cavus M.S. - The Quantum Chemical Calculations of Some Thiazole Derivatives, in: 3rd Int. Conf. Comput. Sci. Technol., 2015.
19. Cui F.Y., Guo L., Zhang S.-T. - Experimental and theoretical studies of 2-amino thiazole as an inhibitor for carbon steel corrosion in hydrochloric acid, Mater. Corros. 65 (2014) 1194–1201.
20. Ongun Yüce A., Doğru Mert B., Kardaş G., Yazıcı B. - Electrochemical and quantum chemical studies of 2-amino-4-methyl-thiazole as corrosion inhibitor for mild steel in HCl solution, Corros. Sci. **83** (2014) 310–316.
21. Döner A., Solmaz R., Özcan M., Kardaş G. - Experimental and theoretical studies of thiazoles as corrosion inhibitors for mild steel in sulphuric acid solution, Corros. Sci. **53** (2011) 2902–2913.
22. Rehan H.H. - 2-Aminothiazole Derivatives as Adsorption Inhibitors for Corrosion of Commercial Copper and Brass in Acid-Solutions, Materwiss. Werksttech. **24** (1993) 304–308.
23. Quraishi M.A., Sharma H.K. - Thiazoles as corrosion inhibitors for mild steel in formic and acetic acid solutions, J. Appl. Electrochem. **35** (2005) 33–39.
24. Perdew J.P., Burke K., Ernzerhof M. - Generalized Gradient Approximation Made Simple, Phys. Rev. Lett. **77** (1996) 3865–3868.
25. Perdew J.P., Burke K., Ernzerhof M. - Errata: Generalized gradient approximation made simple, Phys. Rev. Lett. **78** (1997) 1396.
26. Gece G. - The use of quantum chemical methods in corrosion inhibitor studies, Corros. Sci. **50** (2008) 2981–2992.
27. Frisch M.J., Trucks G.W., Schlegel H.B., Scuseria G.E., Robb M.A., J.R. et al.- Gaussian 09, Revision E.01, Gaussian, Inc., Wallingford CT, 2013.
28. Koopmans T. - Über die Zuordnung von Wellenfunktionen und Eigenwerten zu den Einzelnen Elektronen Eines Atoms, Physica. **1** (1934) 104–113.
29. Chermette H. - Chemical reactivity indexes in density functional theory, J. Comput. Chem. **20** (1999) 129–154.
30. Parr R.G., Chattaraj P.K. - Principle of maximum hardness, J. Am. Chem. Soc. **113** (1991) 1854–1855.
31. Iczkowski R.P., Margrave J.L. - Electronegativity, J. Am. Chem. Soc. **83** (1961) 3547–3551.
32. Yang W., Parr R.G. - Hardness, softness, and the fukui function in the electronic theory of metals and catalysis., Proc. Natl. Acad. Sci. U. S. A. **82** (1985) 6723–6726.
33. Parr R.G., Szentpály L. V., Liu S. - Electrophilicity index, J. Am. Chem. Soc. **121** (1999) 1922–1924.
34. Yang W., Mortier W.J. - The Use of Global and Local Molecular-Parameters for the Analysis of the Gas-Phase Basicity of Amines, J. Am. Chem. Soc. **108** (1986) 5708–5711.
35. Lu T., Chen F. - Quantitative analysis of molecular surface based on improved Marching Tetrahedra algorithm, J. Mol. Graph. Model. **38** (2012) 314–323.
36. Lu T., Chen F. - Multiwfn: A multifunctional wavefunction analyzer, J. Comput. Chem.

33 (2012) 580–592.

37. Obot I.B., Gasem Z.M. - Theoretical evaluation of corrosion inhibition performance of some pyrazine derivatives, Corros. Sci. **83** (2014) 359–366.
38. Khalil N. - Quantum chemical approach of corrosion inhibition, Electrochim. Acta. **48** (2003) 2635–2640.
39. Gece G., Bilgiç S. - Quantum chemical study of some cyclic nitrogen compounds as corrosion inhibitors of steel in NaCl media, Corros. Sci. **51** (2009) 1876–1878.
40. Gao G., Liang C. - Electrochemical and DFT studies of β-amino-alcohols as corrosion inhibitors for brass, Electrochim. Acta. **52** (2007) 4554–4559.
41. Soltani N., Behpour M., Oguzie E.E., Mahluji M., Ghasemzadeh M.A. - Pyrimidine-2-thione derivatives as corrosion inhibitors for mild steel in acidic environments, RSC Adv. **5** (2015) 11145–11162.
42. Oguzie E.E., Enenebeaku C.K., Akalezi C.O., Okoro S.C., Ayuk A.A., Ejike E.N. - Adsorption and corrosion-inhibiting effect of Dacryodis edulis extract on low-carbon-steel corrosion in acidic media, J. Colloid Interface Sci. **349** (2010) 283–292.
43. Şahin M., Gece G., KarcI F., Bilgiç S. - Experimental and theoretical study of the effect of some heterocyclic compounds on the corrosion of low carbon steel in 3.5% NaCl medium, J. Appl. Electrochem. **38** (2008) 809–815.
44. Özcan M., Karadağ F., Dehri I. - Investigation of adsorption characteristics of methionine at mild steel/sulfuric acid interface: An experimental and theoretical study, Colloids Surfaces A Physicochem. Eng. Asp. **316** (2008) 55–61.
45. Obi-Egbedi N.O., Obot I.B., El-Khaiary M.I. - Quantum chemical investigation and statistical analysis of the relationship between corrosion inhibition efficiency and molecular structure of xanthene and its derivatives on mild steel in sulphuric acid, J. Mol. Struct. **1002** (2011) 86–96.
46. Raczyńska E.D., Woźniak K., Dolecka E., Darowska M. - Superbasic properties of the S=N functional group, J. Phys. Org. Chem. **15** (2002) 706–711.
47. Makowski M., Raczyńska E.D., Chmurzyński L. - *Ab Initio* Study of Possible and Preferred Basic Site(s) in Polyfunctional N1 , N1-Dimethyl-N2-cyanoformamidine, J. Phys. Chem. A. **105** (2001) 869–874.
48. Raczyńska E.D., Darowska M., Dąbkowska I., Decouzon M., Gal J.F., Maria P.C. et al. - Experimental and theoretical evidence of basic site preference in polyfunctional superbasic amidinazine: N1,N 1-dimethyl-N2-β-(2-pyridylethyl)formamidine, J. Org. Chem. **69** (2004) 4023–4030.
49. Raczyńska E.D., Makowski M., Górnicka E., Darowska M. - *Ab Initio* Studies on the Preferred Site of Protonation in Cytisine in the Gas Phase and Water, Int. J. Mol. Sci. **6** (2005) 143–156.
50. Ansari K.R., Quraishi M.A., Singh A., Ramkumar S., Obot I.B. - Corrosion inhibition of N80 steel in 15 % HCl by pyrazolone derivatives: electrochemical, surface and quantum chemical studies, RSC Adv. **6** (2016) 24130–24141.